Interference of extracellular soluble algal organic matter on flocculation-sedimentation harvesting of Chlorella sp.

Peer-reviewed author version

LAMA, Sanjaya; PAPPA, Michaela; Brandão Watanabe, Nathalia; Formosa-Dague, Cécile; MARCHAL, Wouter; ADRIAENSENS, Peter & VANDAMME, Dries (2024)
Interference of extracellular soluble algal organic matter on flocculation-sedimentation harvesting of Chlorella sp.. In: Bioresource Technology, 411 (Art N° 131290).

DOI: 10.1016/j.biortech.2024.131290
Handle: http://hdl.handle.net/1942/44357

Journal Pre-proofs

Interference of extracellular soluble algal organic matter on flocculation–sedimentation harvesting of *Chlorella* sp

Sanjaya Lama, Michaela Pappa, Nathalia Brandão Watanabe, Cécile Formosa–Dague, Wouter Marchal, Peter Adriaensens, Dries Vandamme

PII: S0960-8524(24)00994-5
DOI: https://doi.org/10.1016/j.biortech.2024.131290
Reference: BITE 131290

To appear in: *Bioresource Technology*

Received Date: 31 May 2024
Revised Date: 6 August 2024
Accepted Date: 14 August 2024

Please cite this article as: Lama, S., Pappa, M., Brandão Watanabe, N., Formosa–Dague, C., Marchal, W., Adriaensens, P., Vandamme, D., Interference of extracellular soluble algal organic matter on flocculation–sedimentation harvesting of *Chlorella* sp, *Bioresource Technology* (2024), doi: https://doi.org/10.1016/j.biortech.2024.131290

Interference of extracellular soluble algal organic matter on flocculation–sedimentation harvesting of *Chlorella* sp.

Sanjaya Lama[1], Michaela Pappa[1], Nathalia Brandão Watanabe[1, 2], Cécile Formosa–Dague[3], Wouter Marchal[1], Peter Adriaensens[1], Dries Vandamme[1*]

[1] Analytical and Circular Chemistry, Institute for Materials Research (imo-imomec), Hasselt University, Agoralaan Building D, 3590 Diepenbeek, Belgium

[2] Chemical Engineering Department, Escola Politécnica of the University of São Paulo, São Paulo, Brazil

[3] Toulouse Biotechnology Institute, Université de Toulouse, INSA, INRAE, CNRS, Toulouse, France

[*]**Corresponding author:** Dries Vandamme

Email: dries.vandamme@uhasselt.be

Phone: +32 11 26 83 18

Co-authors' Email:

Sanjaya Lama: sanjaya.lama@uhasselt.be

Michaela Pappa: michaela.pappa@uhasselt.be

Nathalia Brandão Watanabe: nbwata@gmail.com

Cécile Formosa–Dague: formosa@insa-toulouse.fr

Wouter Marchal: wouter.marchal@uhasselt.be

Peter Adriaensens: peter.adriaensens@uhasselt.be

Abstract:

Extracellular soluble algal organic matter (AOM) significantly interferes with microalgae flocculation. This study investigated the effects of various AOM fractions on *Chlorella* sp. flocculation using ferric chloride ($FeCl_3$), sodium hydroxide (NaOH), and chitosan. All flocculants achieved high separation efficiency (87–99%), but higher dosages were required in the presence of AOM. High molecular weight (>50 kDa) AOM fraction was identified as the primary inhibitor of flocculation across different pH levels, whereas low/medium molecular weight (<3 and <50 kDa) AOM had minimal impact. Compositional analysis revealed that the inhibitory AOM fraction is a glycoprotein rich in carbohydrates, including neutral, amino, and acidic sugars. The significance of this study is in identifying carboxyl groups (–COOH) from acidic monomers in >50 kDa AOM that inhibit flocculation. Understanding AOM composition and the interaction dynamics between AOM, cells, and flocculants is crucial for enhancing the techno-economics and sustainability of flocculation-based microalgae harvesting.

Acknowledgments

This work was financially supported by the Hasselt University BOF Project (R–9781), Research Foundation Flanders (FWO- Tournesol VS01322N), and FWO- Hercules project AUHL/15/2-GOH3816N. The authors are grateful to all technicians for the execution of IC, HPAEC–PAD, ICP–OES, FTIR, and NMR analyses.

Interference of extracellular soluble algal organic matter on flocculation–sedimentation harvesting of *Chlorella* sp.

Abstract

Extracellular soluble algal organic matter (AOM) significantly interferes with microalgae flocculation. This study investigated the effects of various AOM fractions on *Chlorella* sp. flocculation using ferric chloride ($FeCl_3$), sodium hydroxide (NaOH), and chitosan. All flocculants achieved high separation efficiency (87–99%), but higher dosages were required in the presence of AOM. High molecular weight (>50 kDa) AOM fraction was identified as the primary inhibitor of flocculation across different pH levels, whereas low/medium molecular weight (<3 and <50 kDa) AOM had minimal impact. Compositional analysis revealed that the inhibitory AOM fraction is a glycoprotein rich in carbohydrates, including neutral, amino, and acidic sugars. The significance of this study is in identifying carboxyl groups (–COOH) from acidic monomers in >50 kDa AOM that inhibit flocculation. Understanding AOM composition and the interaction dynamics between AOM, cells, and flocculants is crucial for enhancing the techno-economics and sustainability of flocculation-based microalgae harvesting.

Keywords: Microalgae, Biomass, Dewatering, Ultrafiltration, Heteropolysaccharides

1 Introduction

Microalgae have garnered significant attention as an industrial biomass feedstock due to their potential in producing proteins, carbohydrates, lipids, pigments, and specialty chemicals (Shitanaka et al., 2024). Microalgae-based biorefinery involves several key steps, namely, species-strain selection, cultivation, harvesting, and downstream processing (Qin et al., 2023). Despite general advancements in these steps, efficient and cost-effective harvesting remains a major hurdle for commercializing microalgae-based products (McGrath et al., 2024; Qin et al., 2023). Various solid-liquid separation methods, such as centrifugation, screening, filtration, gravity sedimentation, flocculation, flotation, etc., have been explored for microalgae harvesting (Liu et al., 2023). Among these, flocculation-based methods as a primary dewatering step are particularly promising due to their energy efficiency and scalability (Liu et al., 2023; McGrath et al., 2024). However, the effectiveness of flocculation is influenced by several factors, including species type, cell morphology, medium composition, ionic strength, pH, etc. (Henderson et al., 2008; Lama et al., 2016). Moreover, a key determinant of the economic viability of flocculation is the type, cost, and dosage of flocculants used (Liu et al., 2023). Thus, a fundamental understanding of interaction dynamics between microalgal cells, flocculants, and medium components is crucial.

One of the critical medium components affecting the microalgal flocculation process is the extracellular algal organic matter (AOM) (Cheng et al., 2024; Zang et al., 2020; Zhang et al., 2024). AOM is a complex mixture of organic compounds released by algal cells, predominantly composed of polysaccharides (up to 88%) and proteins (up to 67%) with a net negative charge (Naveed et al., 2019; Zhou et al., 2024). Previous studies have demonstrated that AOM can inhibit flocculation by competing with cells for positively charged flocculants (Cheng et al., 2022; Pivokonsky et al., 2012; Zang et al., 2020). Some studies have shown that the extensive network of AOM may induce the bridging of cells in the presence of positively charged flocculants (Cheng et al., 2024; Vu et al., 2021; Zhang et al., 2024). Nevertheless, its specific role in flocculation–based microalgal biomass harvesting remains insufficiently explored. Hence, detailed AOM compositional analysis could provide further insights into the interaction mechanism of AOM, cells, and flocculants (Rao et al., 2020; Yang et al., 2020). Understanding the quantity and composition of AOM and its potential interference with different flocculation methods will offer valuable insights for selecting effective flocculants. Moreover, identifying the active functional groups in AOM can render new avenues for utilizing AOM as a flocculant aid or *in situ* flocculating agent, with positive implications for the economic viability and environmental sustainability of microalgae biomass production. This study focuses on understanding the interference of AOM in the flocculation of *Chlorella* sp., which produces a substantial quantity of AOM during the early stationary phase. Unlike previous studies that broadly address the impact of AOM, this study breaks down AOM into specific molecular weight (MW) fractions via sequential ultrafiltration and investigates their roles in unique flocculation mechanisms induced by ferric chloride ($FeCl_3$), sodium hydroxide (NaOH), and chitosan. A comprehensive analysis of AOM composition was achieved by employing advanced, sample non-destructive techniques, such as Fourier transform infrared spectroscopy (FTIR) and solid-state ^{13}C-NMR spectroscopy, which pinpointed functional groups that interfere with flocculation. This innovative approach provides valuable insights into the interactions between AOM and flocculants under various pH conditions, paving the way for improved microalgae harvesting strategies. The results of this study not only advance the understanding of AOM's role in flocculation but also propose tailored approaches to enhance flocculation efficiency in microalgal biomass recovery.

2 Materials and methods

2.1 Cultivation of *Chlorella* sp.

Freshwater green microalga *Chlorella* sp. (kindly provided by Ecotoxicology and Environmental Services Laboratory of the National Center of Applied Electromagnetism, Universidad de Oriente, Cuba) was cultivated in nitrate-modified (100 mg·L^{-1} NO_3^-) BG-11 medium prepared with sterilized deionized water (Wu et al., 2012). The cultivation was done in two identical bubble column photobioreactors (25 L, length × diameter: 100 cm × 20 cm) at room temperature (20±2 °C). The culture was mixed using 0.2 µm filtered air (2 L min^{-1}), with the pH maintained at 8.50 by dosing pure pressurized CO_2 via pH-controller system (DENNERLE, pH-Controller Evolution DeLuxe). Each photobioreactor was illuminated on two opposite sides with LED lights (7000K- daylight, 4000K-warm white, and RGB colored 1200 mm GoldLine LED, HVP Aqua) in a 16:8 h light: dark cycle, providing a photon flux density of approximately 150 µmol photons m^{-2} s^{-1} at the reactor surface. Culture growth was monitored by measuring optical density at 750 nm (OD_{750}) using a UV–visible spectrophotometer (Ultraspec–7000). The OD_{750}-based growth curve was fitted with a growth sigmoidal function (Sigmoidal Logistics Function, Origin 2020) (Ajala & Alexander, 2020). Additionally, OD_{750} was calibrated (linear fit) against microalgal dry weight (DW) biomass concentration (g L^{-1}), which was determined gravimetrically. This involved filtering a known volume of culture on pre-weighed glass microfiber filters (Whatman GF6, 47 mm diameter) and drying overnight at 105°C. Overall, 50 L of culture (from 2×25 L photobioreactors) was consumed during the experimental procedure.

2.2 Isolation of extracellular soluble algal organic matter (AOM)

The culture at any growth phase from the photobioreactor is referred to hereafter as a culture with extracellular soluble algal organic matter (AOM), designated as AOM+ culture. A culture suspension without AOM, designated as AOM− culture, was prepared by resuspending centrifuged cell pellets in fresh nitrate-modified BG-11 medium (Vandamme et al., 2016). Cell/debris-free culture supernatant obtained after centrifugation of AOM+ culture is referred to as extracellular soluble algal organic matter (AOM**)** (Figure 1) (Rao et al., 2020). Centrifugation was performed at 8000 rpm (~5000 ×*g*) (FJ 130 EPR, Milky Day, Czech Republic) and repeated 2-3 times until the supernatant was cell/debris-free. Approximately 20 L of AOM was isolated from the early stationary phase (day 15) culture for fractionation (ultrafiltration) to obtain different MW fractions for the flocculation experiments. AOM was collected during the early stationary phase, when cell growth slowed, but cell lysis and release of intracellular or cell wall components were minimal. Thus, AOM isolated mainly comprises cell-secreted or surface-dissociated dissolved/soluble extracellular organic matter (Rao et al., 2020; Villacorte et al., 2015; Vu et al., 2021).

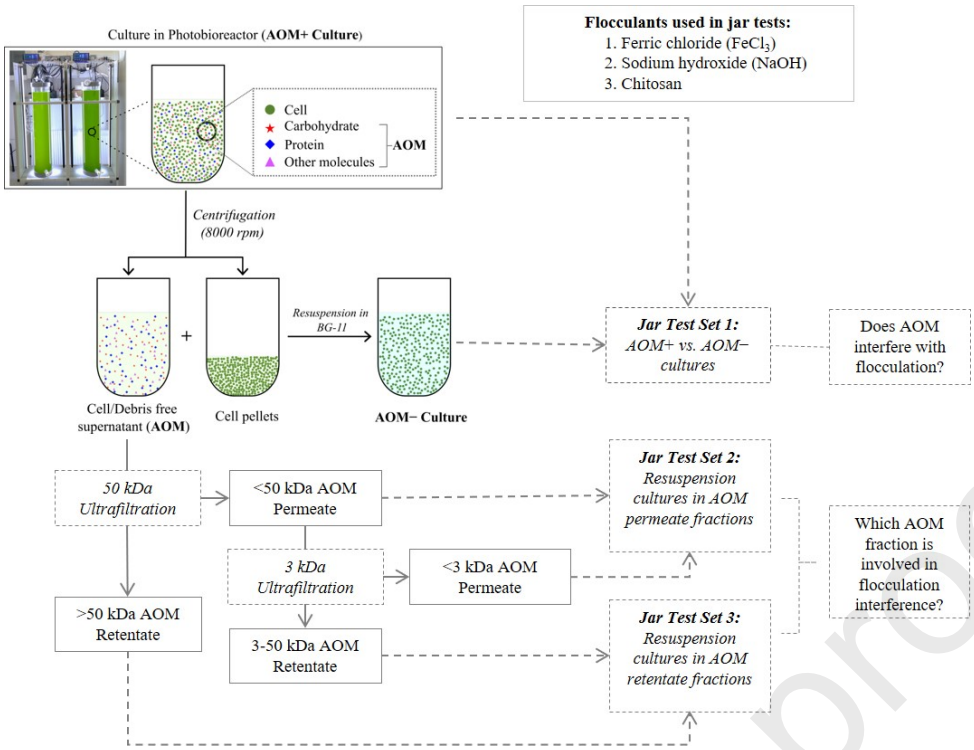

Figure 1: Experimental overview for AOM isolation, fractionation and flocculation jar tests for various culture suspensions: AOM+, AOM−, and AOM fractions resuspension cultures.

2.3 Ultrafiltration of algal organic matter (AOM)

Ultrafiltration of AOM (20 L, day 15) was conducted using a tangential flow filtration system (ÄKTA flux 6, Cytiva). The first ultrafiltration step employed a hollow–fiber filter cartridge with a nominal molecular weight cut–off (NMWCO) of 50 kDa and a membrane area of 0.14 m^2 (UFP–50–C–4X2MA, Cytiva). This process operated at constant transmembrane pressure (TMP) of 60 kPa in retentate recycle mode, concentrating the feed AOM solution 36-fold. The <50 kDa AOM permeate fraction (~18 L) from this step was divided, with 10 L used for further ultrafiltration with a 3 kDa filter and 8 L stored at 4°C for flocculation resuspension jar tests (set 2). The second ultrafiltration of <50 kDa AOM permeate fraction was performed with a 3 kDa NMWCO filter (UFP–3–C–4X2MA, membrane area of 0.14 m^2, Cytiva) at 70 kPa TMP, concentrating the feed solution 21-fold. The <3 kDa AOM permeate fraction (~8 L) was collected and stored at 4°C until further use in the flocculation resuspension jar tests (set 2). Concentrated AOM retentate fractions (>50 kDa and 3–50 kDa) from each ultrafiltration were dialyzed with distilled water until the water permeate conductivity (inoLab Cond 7110) decreased from 650 µS cm^{-1} to less than 20 µS cm^{-1}. Approximately half of the concentrated liquid AOM (>50 kDa fraction) was lyophilized for 48 h at –40°C under 12 Pa vacuum pressure (CHRIST, ALPHA 1–2 LDPlus). This process yielded 1.36 g L^{-1} of lyophilized >50 kDa AOM. Both lyophilized and remaining liquid AOM fractions were stored at –20°C until further use in analysis and jar tests (set 3) with AOM retentate fraction.

2.4 Total organic carbon, total nitrogen, and elemental composition

The total organic carbon (TOC), measured as non-purgeable organic carbon, and total nitrogen (TN) in AOM were assessed daily during the culture growth using a TOC analyzer (TOC–L_{CPH}, Shimadzu Benelux). The concentrations of readily available elements (Al, B, Ca, Fe, K, Mg, Mn, Na) were determined with an inductively coupled plasma optical emission

spectrometer (ICP–OES) (Perkin Elmer Optima 8300). Anions (NO_3^-, NO_2^-, Cl^-, PO_4^{3-}, SO_4^{2-}) were measured by ion chromatography (Thermo Scientific Dionex ICS–6000) using Dionex IonPac AS14A column (4x250 mm).

2.5 Flocculation experiments

2.5.1 Flocculant stock solutions

Fresh stock solutions of 10 g·L^{-1} ferric chloride (Merck) and 0.5 M sodium hydroxide (Sigma–Aldrich) were prepared in Milli–Q water. Chitosan (MW: 100–300 kDa, Acros Organics) stock of 5 g·L^{-1} was prepared in 0.04 M of HCl (VWR Chemicals) by rapidly mixing (500 rpm) the solution mixture for 1.5 h.

2.5.2 Jar test procedure

All the jar tests were performed with microalga culture suspension maintained at an equivalent dry biomass concentration of 0.60±0.05 g·L^{-1} and an initial pH of 8.50±0.15 at room temperature (20±2°C). Culture suspension (100 mL) was distributed in a series of 10–15 transparent plastic jars (VWR, 216–1830) placed over a multi-position magnetic stirrer (IKA RO 15). Each flocculant stock solution was added to the culture suspensions to achieve a final concentration of 0–1000 mg·L^{-1}. For NaOH flocculation jar test, 10 mM of magnesium chloride hexahydrate (VWR Chemicals BDH) was added to a culture suspension before sodium hydroxide dosing (Fan et al., 2017; Vandamme et al., 2016; Wu et al., 2012). During flocculant addition, culture suspensions were vigorously mixed at 350 rpm for 10 minutes, followed by gentle mixing at 250 rpm for 20 minutes. The pH of each jar (measured with a Knick pH–Meter 764 Multi-Calimatic) was noted at the end of the rapid mixing phase. After mixing, suspensions were allowed to settle for 30 min, and 3.3 mL samples were collected from approximately 1.5 cm below the suspension surface for optical density (OD_{750}) measurement. The separation efficiency (SE %) for each treatment was estimated using Eq. (1):

$$\text{Separation Efficiency (SE \%)} = \frac{\mathrm{OD_i} - \mathrm{OD_f}}{\mathrm{OD_i}} \times 100 \qquad (1)$$

Where OD_i and OD_f are OD_{750} measurements before flocculant addition and after settling, respectively (Lama et al., 2016; Vandamme et al., 2012). Based on the resulting series of SE (%) achieved against applied dosage (mg g^{-1} of dry biomass), dose-response curve fitting was performed by using a sigmoidal regression model (Boltzmann function, Origin 2020). The model is defined in Eq. (2) as follows (Lama et al., 2016; Zhang et al., 2012):

$$y = A_2 + \frac{A_1 - A_2}{1 + e^{\left(\frac{x - x_0}{dx}\right)}} \qquad (2)$$

where y is response value (SE %) depending on flocculant dosage (x). Flocculant dosage at the inflection point (x_0)—a midpoint of the sigmoidal curve—represents the minimum dosage required to induce flocculation. A slope factor (dx) at the inflection point determines a curve's steepness and, thus, the sensitivity of the SE to the flocculant dosage. For high dx, increase in SE is slow, while for low dx, increase is rapid. A_1 and A_2 are the response values (SE %) corresponding to the asymptotes on the minimum and maximum boundaries of the curve. Additionally, the optimum flocculant dosage— minimum dosage corresponding to the maximum SE (A_2)— was used as a reference dosage in subsequent jar tests.

2.5.3 Jar test on cultures with (AOM+) and without (AOM−) AOM (Jar test set 1)

The effect of AOM in the flocculation process was assessed by jar tests on AOM+ and AOM− culture suspensions (day 18 culture, DW=0.63 $g \cdot L^{-1}$, pH 8.50). AOM− culture was prepared by resuspension of centrifuged AOM+ culture cells pellet in fresh BG-11 medium. A desired biomass concentration in resuspension was maintained by adjusting OD_{750} with reference from the OD_{750} *vs.* DW linear fit ($DW = 0.2776 \pm 0.0044 \times OD_{750} - 0.0229 \pm 0.0076$, $R^2 = 0.98$). Jar tests were carried out as detailed in the jar test procedure.

2.5.4 Jar test on AOM permeate resuspension cultures (Jar test set 2)

Flocculation jar tests (as detailed in the jar test procedure) were performed on AOM+, AOM−, <50 kDa, and <3 kDa resuspension cultures to evaluate the effect of low/medium MW (<3 and <50 kDa) AOM permeate fractions. AOM and its fractions used in this test were processed in advance using the early stationary phase (day 15) culture, as detailed in the AOM isolation and ultrafiltration section. Centrifuged cells (day 19) were resuspended in AOM (day 15), fresh BG-11 medium, <50 kDa and <3 kDa AOM permeate fractions to make AOM+, AOM−, <50 kDa, and <3 kDa AOM culture suspensions (0.60 $g \cdot L^{-1}$, pH 8.50). The flocculation jar tests were conducted following the procedure detailed in the jar test protocol.

2.5.5 Jar test on AOM retentate resuspension cultures (Jar test set 3)

The effect of high MW (>50 kDa) AOM fraction in the flocculation was determined by performing resuspension jar tests with >50 kDa AOM retentate fraction (liquid, 36-fold concentrated, lyophilized yield of 1.36 g L^{-1}) obtained in the ultrafiltration section. A slight modification was made to the jar test procedure before the addition of flocculant stocks. Liquid AOM (concentrated >50 kDa fraction) was added in increasing concentrations (equivalent TOC concentrations of 0–35 mg L^{-1}) to the AOM− culture suspension (0.60 $g \cdot L^{-1}$, pH 8.50). During the addition of the AOM fraction, the culture suspension was homogeneously mixed at 400 rpm for 5 minutes. Flocculant stocks were added to attain a final concentration of 135.0, 235.0, and 65.0 mg g^{-1} dry biomass of $FeCl_3$, NaOH, and chitosan, respectively. These flocculant dosages correspond to optimum dosages, which achieved maximum separation efficiencies (≥98 %) in AOM− culture jar test set 1. Following the addition of flocculants, all procedures were carried out as outlined in the jar test procedure.

2.6 Compositional analysis of >50 kDa AOM fraction

2.6.1 Fourier–transform infrared (FTIR) spectroscopy

Fourier–transform infrared (FTIR) spectroscopy of lyophilized >50 kDa AOM (day 15 AOM obtained as detailed in the ultrafiltration section) was performed with a Vertex 70 spectrometer equipped with a deuterated triglycine sulfate (DTGS) detector (Bruker, Karlsruhe, Germany) in attenuated total reflection (ATR) mode using a diamond crystal (PIKE, Fitchburg, USA). Thirty-two scans per sample were obtained in the 4000–600 cm^{-1} spectral region at a resolution of 4 cm^{-1}. Baseline correction and normalization were performed on the largest peak, which varied for each sample. Band assignments were made following numerous reference studies (Capek et al., 2008; Cybulska et al., 2016; Liu et al., 2021; Pinel et al., 2020; Villacorte et al., 2015).

2.6.2 Solid–state ^{13}C–Nuclear magnetic resonance (NMR) spectroscopy

Solid-state ^{13}C–CP/MAS (Cross Polarization/Magic Angle Spinning) NMR experiments were performed on a Varian VNMRS 400 MHz spectrometer (9.4 T, Agilent) using a T3HX 3.2 mm VT probe. Lyophilized >50 kDa AOM (80 mg, day 15 AOM obtained as detailed in the ultrafiltration section) was introduced into airtight ceramic zirconia rotors of 3.2 mm in diameter (22 µL rotors). Spectra were recorded with a MAS spinning frequency of 15 kHz at 25 °C. The aromatic signal of hexamethylbenzene was used to determine the Hartmann–Hahn condition for cross-polarization and to calibrate the carbon chemical shift scale (132.1 ppm). Acquisition parameters were as follows: a spectral width of 50 kHz, a 90° pulse length of 2.5 µs, a contact time for cross-polarization of 1.0 ms, an acquisition time of 20.0 ms, a recycle delay time of 2.5 s, and approximately 30,000 scans. High–power proton dipolar decoupling during the acquisition time was set to 85 kHz (Arnold et al., 2015). Spectra were processed using Delta software (version 6.3.0, Jeol).

2.6.3 Total carbohydrate, total protein, and monosaccharide composition

AOM stock solution was prepared by dissolving 5 mg of lyophilized >50 kDa AOM (day 15 AOM obtained as detailed in the ultrafiltration section) in 5 mL of Milli–Q water under continuous stirring overnight at 4°C. For acid hydrolysis, 100 µL AOM stock solution was transferred to screw–cap Pyrex tubes and dried under a nitrogen stream. Then, 1 mL of 3 M Methanolic HCl (Merck) was added to the dried tube and incubated at 95°C for 3 h, followed by cooling in an ice bath for 5 minutes and subsequent drying under a nitrogen stream at 25°C. The second hydrolysis step involved adding 1 mL of 2 M trifluoroacetic acid (Merck), followed by heating at 121°C for 1 h and drying under a nitrogen stream (Nagel et al., 2014). The dried hydrolysate was resuspended with 2 mL of Milli–Q water. Any further dilution required was done with Milli–Q and filtered (Nylon 0.22 µm) before analysis. Total carbohydrate content was determined with 500 µL of hydrolysate using the 3-methyl-2-benzothiazolinone hydrazone (MBTH) method, with D–glucose (Sigma, BioXtra, ≥99.5 %) as standard (Van Wychen & Laurens, 2016). Total protein was quantified with 500 µL of aliquots using a Pierce BCA Protein Assay Kit (Thermo Scientific, Product: 23227).

Monosaccharide composition was analyzed using a high–performance anion–exchange chromatography system with pulsed amperometric detection (HPAEC–PAD) (Thermo Scientific Dionex ICS–6000). The system included a CarboPac PA20 guard column (3 × 50 mm) and a CarboPac PA20 analytical column (3 × 150 mm) maintained at 20°C. The detector was equipped with a non-disposable gold working electrode and palladium hydrogen (PdH) reference electrode, applying the standard carbohydrate quadrupole–potential waveform (Chromeleon software version 7.3.1). The autosampler was set for a full loop sample injection volume of 25 µL at a flow rate of 0.4 mL/min. The eluent consists of four different channels, namely: A: Milli–Q water, B: 10 mM sodium hydroxide (NaOH) + 10 mM sodium acetate (NaAce), C: 100 mM NaOH + 100 mM NaAce, and D: 100 mM NaOH. The following gradient was applied: 0–25 min 94 % A; 5 % B, 1% D; 25–27 min 45 % A; 5 % B, 50% D; 27–46 min 100 % C; 46–50 min 100 % D; 50–60 min 94 % A; 5 % B, 1% D. Detection and quantification of analytes were done by using calibration standards (0.1, 0.2, 0.5, 0.8, 1.0, 2.0, 3.0, 4.0 $\mu g \cdot mL^{-1}$) of 12 mixed monosaccharides: neutral (fucose, rhamnose, arabinose, galactose, glucose, xylose, mannose, and ribose); amino (galactosamine and glucosamine); and acidic (galacturonic acid and glucuronic acid). The total carbohydrate, protein, and monomer composition were expressed as weight percentage (wt %) of the lyophilized >50 kDa AOM sample.

2.7 Statistical Analysis

In addition to sigmoidal regression for all dose-response results, one-way ANOVA followed by Tukey's mean comparison test (Origin 2020) was performed to evaluate the significance differences ($p<0.05$) among the results obtained on separation efficiencies, dosages, TOC concentrations of AOM+, AOM−, and resuspension cultures. The analytical results represent the average of triplicate measurements.

3 Result and discussion

3.1 Culture growth characteristics

Culture growth was monitored daily by measuring optical density (OD_{750}) and dry weight (DW) (Figure 2A). Biomass DW followed a similar trend to OD_{750} (Linear fit: DW = 0.2776±0.0044×OD_{750} − 0.0229±0.0076, R^2 = 0.98) over the growth period, attaining 0.6–0.7 $g \cdot L^{-1}$ during jar test experimental days (day 15–20). A midpoint of the OD_{750}-based growth curve indicates a mid-exponential phase around day 7. The stationary phase began on day 14 and lasted until day 30, with no observed decline phase. On the inoculation day, medium nitrate (NO_3^-) and phosphate (PO_4^{3-}) levels were 91.4±1.3 $mg \cdot L^{-1}$ and 20.0±0.3 $mg \cdot L^{-1}$, respectively, and they depleted to <2.5 $mg \cdot L^{-1}$ and 8.6±1.5 $mg \cdot L^{-1}$ on day 7, corresponding to mid-exponential growth phase in OD_{750} based growth curve. Additionally, total organic carbon (TOC) in the extracellular soluble algal organic matter (AOM) increased throughout the growth period—from 5.1±1.4 $mg \cdot L^{-1}$ on inoculation day to 27.8±3.2 $mg \cdot L^{-1}$ on day 18—indicating the accumulation of organic matter in the culture (Vu et al., 2021; Zhang et al., 2012). However, total nitrogen (TN) in the AOM decreased over time, from 20.5±0.2 $mg \cdot L^{-1}$ on inoculation day to <2.0 $mg \cdot L^{-1}$ on day 7 onwards (Figure 2B). TN measured on inoculation day can be attributed to the culture medium nitrate ($N–NO_3^-$). Rapid decrease in TN over the growth period is consistent with medium nitrate depletion due to assimilation by growing cells (Ajala & Alexander, 2020). Overall, culture growth in both photobioreactors was consistent and replicable in terms of OD_{750}, DW, NO_3^-, PO_4^{3-}, TOC, and TN measurements.

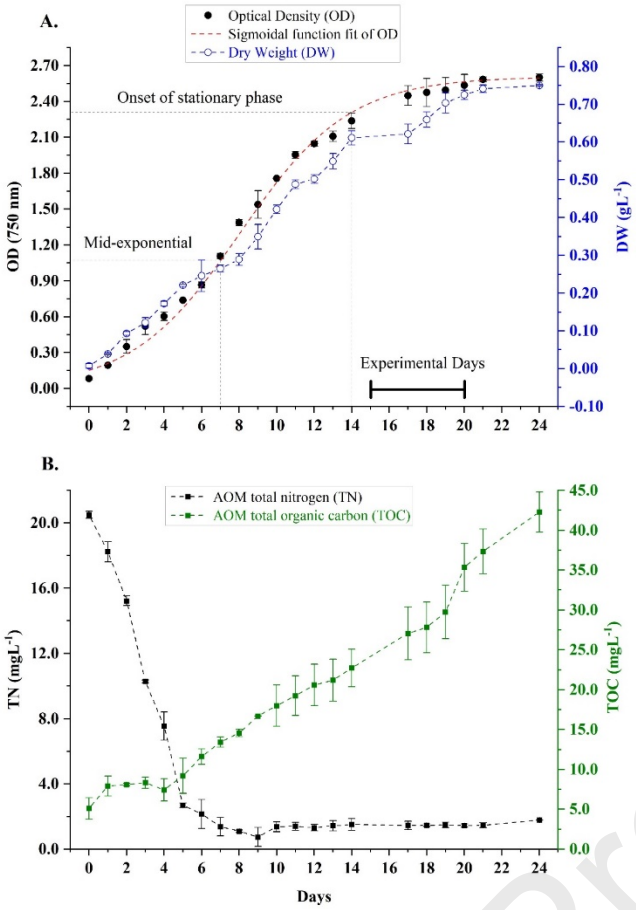

Figure 2: A: Growth curve of *Chlorella* sp.; OD values are fitted (Red dashed curve) with a sigmoidal function to observe growth phases. **B:** TN and TOC levels in AOM throughout growth.

3.2 Interference of total algal organic matter (AOM) in flocculation (Jar test set 1)

The effect of total/whole AOM in the flocculation was evaluated by jar test on early stationary phase (day 18) AOM+ and AOM− cultures using three flocculants: $FeCl_3$, NaOH, and chitosan. A sigmoidal dose-response model of the separation efficiency (SE %) against the flocculant dosage was a good fit with the experimental data ($R^2 > 0.99$). The inflection point dosage (x_0) was used to compare dose responses of AOM+ and AOM− cultures (Figure 3). Additionally, the optimum flocculant dosage ($mg \cdot L^{-1}$) corresponding to the maximum SE (A_2 in sigmoidal regression) for each flocculant is presented in Table 1. For all sigmoidal regression fitting, p-values for the t-test of parameters A_2 and x_0 were statistically significant ($p<0.001$), indicating that these parameters are unlikely to be zero. The optimum flocculant dosages obtained here are selected as a reference dosage for further jar tests.

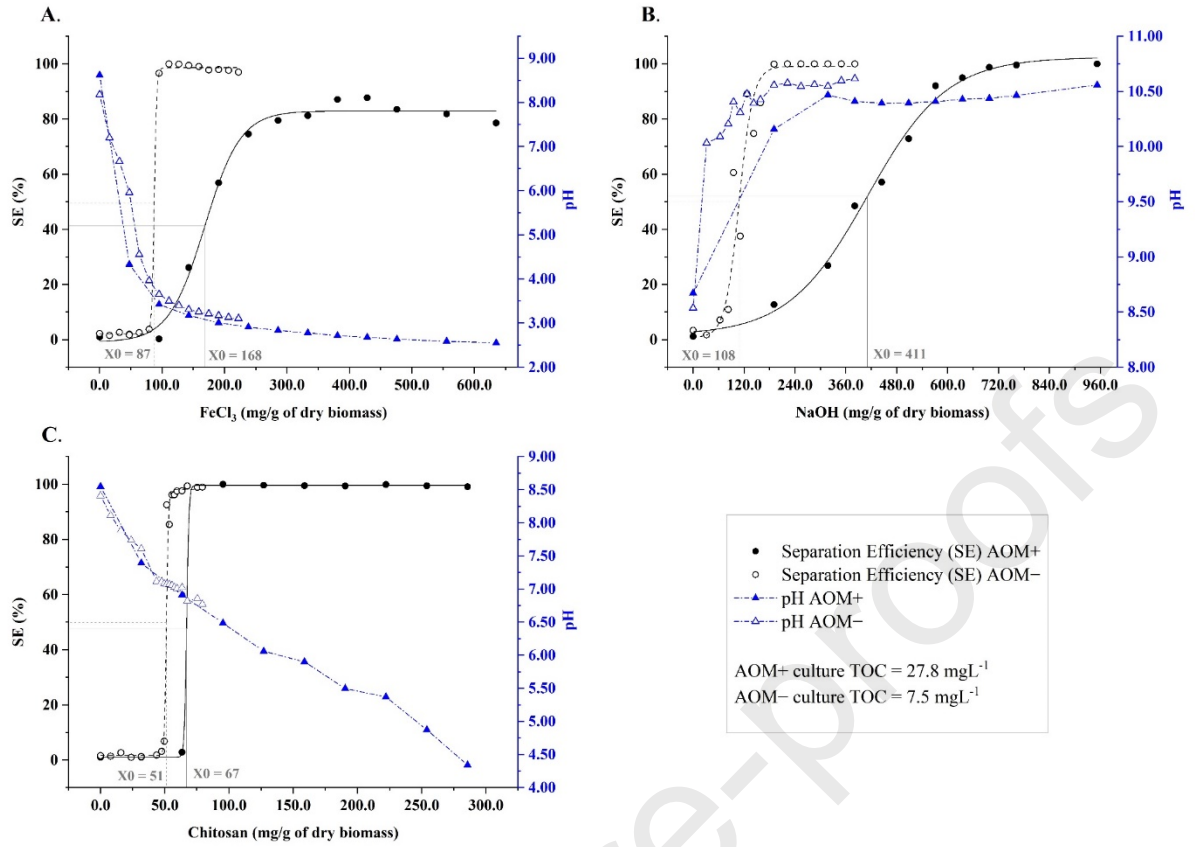

Figure 3: Dose-response curves (SE% corresponding to an applied dosage of **A.** $FeCl_3$, **B.** NaOH, and **C.** Chitosan) from sigmoidal regression of AOM+ *vs.* AOM− culture jar tests (Jar test set 1). Final pH values corresponding to applied dosages are represented on the right axis (blue). Highlighted values indicate the inflection point dosages (x_0) corresponding to grey dashed droplines.

Flocculation was successful for all three flocculants, achieving SE above 97%, except for the $FeCl_3$ in the AOM+ culture, which achieved 87%. The significant difference ($p<0.05$) in dose-response between AOM+ and AOM− cultures is clearly observed in the inflection point dosage (x_0). Since flocculant dosage is crucial in determining the final cost of flocculation-based harvesting, even the small change in x_0 and, consequently, the optimum dosage should not be overlooked (Lama et al., 2016; McGrath et al., 2024). A variation (% decrease) of x_0 in AOM+ versus AOM− culture is highest for NaOH (74%), followed by $FeCl_3$ (48%) and chitosan (23%). Prevalence of organic matter in AOM+ culture is indicated by significantly higher TOC concentrations (27.8±3.2 mg·L^{-1}) compared to AOM− culture (7.5±0.8 mg·L^{-1}) and BG-11 medium (1.43±0.12 mg·L^{-1}). Thus, the disparity observed in the flocculation dose-response can be attributed to the presence of organic matter, represented in this study as AOM, which is consistent with previous studies (Beuckels et al., 2013; Chen et al., 2009; Garzon-Sanabria et al., 2013; Wu et al., 2012; Zang et al., 2020; Zhang et al., 2012).

Table 1: Optimum flocculant dosage (minimum dosage corresponding to maximum SE%), final pH, and sigmoidal regression parameters (x_0, dx) from AOM+ *vs.* AOM− culture dose-response curves (for each sigmoidal regression, R^2 =1.00).

Flocculants	$FeCl_3$		NaOH		Chitosan	
Culture*	**AOM+**	**AOM−**	**AOM+**	**AOM−**	**AOM+**	**AOM−**
Dosage (mg g^{-1} of dry biomass)	404.8±33.7	119.0±11.2	730.2±44.9	206.3±22.4	111.1±22.4	61.5±2.8
Dosage (mg·L^{-1})	255.0±21.2	75.0±7.1	460.0±28.3	130.0±14.1	70.0±14.1	38.8±1.8
Maximum SE (%)	87	99	99	99	99	98
Final pH	2.70±0.03	3.45±0.07	10.45±0.02	10.57±0.01	6.27±0.30	6.89±0.01
x_0 (mg g^{-1} of dry biomass)	168.1±5.2	87.4±1.0	410.5±11.6	108.0±5.8	67.0±0.4	51.3±0.5
Slope factor, *dx*	28.7±4.3	2.0±0.3	93.3±11.1	16.5±4.3	0.9±0.0	0.8±0.2

*Culture properties: Initial pH = 8.50, Dry weight = 0.63 g·L^{-1}, AOM+ culture TOC = 27.8±3.2 mg·L^{-1}, AOM− culture TOC = 7.5±0.8 mg·L^{-1}

In the case of $FeCl_3$ flocculation, the optimum dosage is significantly higher for AOM+ culture (405 mg g^{-1} dry biomass) than for AOM− culture (119 mg g^{-1}). The higher dosage requirement for AOM+ culture is also reflected by the slope of the dose-response curve (Figure 3A). From sigmoidal regression, slope factors (*dx*) of 28.71 and 2.01 were obtained for AOM+ and AOM− culture, respectively (Table 1). A large *dx* indicates lower sensitivity of the sigmoidal curve, requiring higher dosage change to achieve a quick shift in SE. Conversely, in a higher sensitivity (*dx* approaching 1) sigmoidal curve, SE changes rapidly with small dosage increments, as observed for the AOM− dose-response curve (Figure 3A). During $FeCl_3$ flocculation, dissolved iron species (such as Fe^{3+}, $Fe(OH)^{2+}$, and $Fe(OH)_2^{+}$) and ferric hydroxide precipitate ($Fe(OH)_3$) surfaces are cationic at pH < 8.0 (Wyatt et al., 2012). In the pH range from 4.1 to 8.0, $Fe(OH)_2^{+}$ is the predominant species in equilibrium with positively charged ferric hydroxide precipitate (Johnson & Amirtharajah, 1983). Positively charged precipitates induce flocculation by bridging negatively charged cells together through an electrostatic patch mechanism (Wyatt et al., 2012). Whereas, at high cell concentrations (> 0.5 g·L^{-1}), flocculation is induced by the combination of electrostatic bridging and sweep flocculation (Kim et al., 2015; Wyatt et al., 2012). The higher dosage requirement for AOM+ culture could be attributed to the metal complexation properties of AOM, making cationic hydrolyzed species less available for interaction with cells (Chen et al., 2009; Naveed et al.,

2019). Since culture pH is not adjusted during the flocculation experiment, $FeCl_3$ hydrolysis releases hydrogen ions into the culture suspension, causing the pH to decrease from 8.50 to 2.70–3.45 (Table 1). For both AOM+ and AOM− cultures, the pH decreases sharply with increasing $FeCl_3$ dosage up to ~130 mg g^{-1} and then shows a plateau at higher dosages (Figure 3A). As observed in previous studies, the final pH corresponding to the maximum SE for both cultures is in the acidic range of 2.70–3.45 (Kim et al., 2015).

For NaOH/alkaline flocculation, optimum NaOH dosage at maximum SE (99 %) is 3.5 times higher in the AOM+ culture compared to the AOM− culture. The dose-response curves displayed a trend similar to that observed in $FeCl_3$ flocculation. The large slope factors (*dx* = 93.32 AOM+ and 16.48 for AOM− cultures) indicate lower sensitivity, requiring higher dosage changes to attain rapid variations in SE (Figure 3B). Since the final pH required to achieve maximum SE for both cultures reaches around 10.50 (Table 1), a larger quantity of NaOH was consumed to reach this pH for the AOM+ culture. This is demonstrated by the swift rise in pH with a small NaOH dosage increment in the AOM− culture (Figure 3B). The presence of AOM consumed a significant amount of hydroxide (OH^-) to reach pH 10.50, necessitating additional hydroxide to form $Mg(OH)_2$ precipitates in the AOM+ culture (Besson & Guiraud, 2013; Li et al., 2021; Vandamme et al., 2016). Optimum pH of ≥ 10.50 is reported to be critical for forming gelatinous, positively charged $Mg(OH)_2$ precipitates, which induce flocculation by charge neutralization and sweep flocculation (Brady et al., 2014; Vandamme et al., 2016). Additionally, Mg^{2+} ions adsorbed on the cell surface at high pH could provide the nucleation sites for $Mg(OH)_2$ precipitates around the cell, thus enhancing flocculation (Brady et al., 2014; Li et al., 2021). Alkaline pH above 8.50 can also facilitate the formation of calcium phosphate precipitates, promoting sweep flocculation at high concentrations of Ca^{2+} (0.85 mM) and PO_4^{3-} (0.35 mM) (Beuckels et al., 2013; Brady et al., 2014). However, low concentrations of Ca^{2+} (0.24 mM) and PO_4^{3-} (0.05 mM) in this study rule out this possibility. Moreover, at a pH range of 10.50, dominant surface functional groups such as carboxyl (pK_a 2–6), phosphoryl (pK_a 5.6-7.2), and hydroxyl (pK_a 8–12) may remain fully deprotonated (Brady et al., 2014), explaining the relatively high NaOH dosages required compared to $FeCl_3$ (Figure 3) (Wu et al., 2012).

Among the three flocculants, chitosan performed the most efficiently, achieving SE ≥98% at the lowest concentrations of 111 mg g^{-1} dry biomass for AOM+ and 62 mg g^{-1} for AOM− culture. Consistent with $FeCl_3$ and NaOH flocculation, a higher dosage was required for AOM+ culture compared to AOM− culture. However, the optimum dosage difference between AOM+ and AOM− cultures was minimal. At pH 8.0, it is proposed that no specific/electrostatic interaction occurs between chitosan and cells, and flocculation is primarily induced by a sweeping mechanism (Demir et al., 2020). Thus, the minimal dosage difference observed for AOM+ and AOM− cultures could be attributed to the dominant sweeping mechanism. However, the higher dosage requirement for AOM+ culture, possibly due to intermolecular interaction between chitosan (pK_a ~ 6.5) and deprotonated carboxyl/phosphoryl functional groups in AOM, should not be neglected (Garzon-Sanabria et al., 2013; Zang et al., 2020). Additionally, the sensitivity of the chitosan dose-response curve is approximately identical for both cultures (slope factors, *dx* = 0.88 for AOM+ and 0.80 AOM−) and significantly better (*dx* approaching 1) than those observed for $FeCl_3$ and NaOH (Figure 3). pH decrease of both cultures with increasing chitosan dosages follows a consistent trajectory, arriving at a final pH of 6.27 (AOM+) and 6.89 (AOM−) at the maximum SE. Overall, despite the unique mechanism of each flocculant studied, the need for higher dosage is prominent in the presence of AOM. Consequently, further jar tests were conducted to determine the specific AOM fraction accountable for the inhibition.

3.3 Interference of AOM permeate fractions in flocculation (Jar test set 2)

Sequential ultrafiltration produced two different AOM permeate fractions (8.0 L each): <50 kDa fraction of low/medium MW and <3 kDa fraction of low MW. Jar tests (set 2) evaluated culture suspensions prepared with different AOM fractions: AOM+, AOM−, <50 kDa, and <3 kDa AOM. A maximum SE of ≥ 97% was achieved for all the culture suspensions (Figure 4, first row). The general trend of requiring higher dosage for AOM+ compared to AOM− culture was analogous to the previous jar test set 1 (Figure 3). The optimum dosages and inflection point dosages (x_0) for AOM+ and AOM− cultures are relatively proportional to those in jar test set 1, except for chitosan, which exhibited slightly higher values (p<0.05) (see supplementary material, Table S1). The pH response of the culture suspensions to applied flocculant dosages displayed a comparable progression to that in jar test set 1 (Figure 4, second row). The final pH range corresponding to the maximum SE was 3.41–3.89 for $FeCl_3$, 10.39–10.44 for NaOH, and 6.97–7.27 for chitosan (see supplementary material, Table S1). The marginal disparity (p<0.05) in optimum dosages and final pH values for AOM+ and AOM− culture compared to jar test set 1 could be attributed to the cells and AOM being at different growth days.

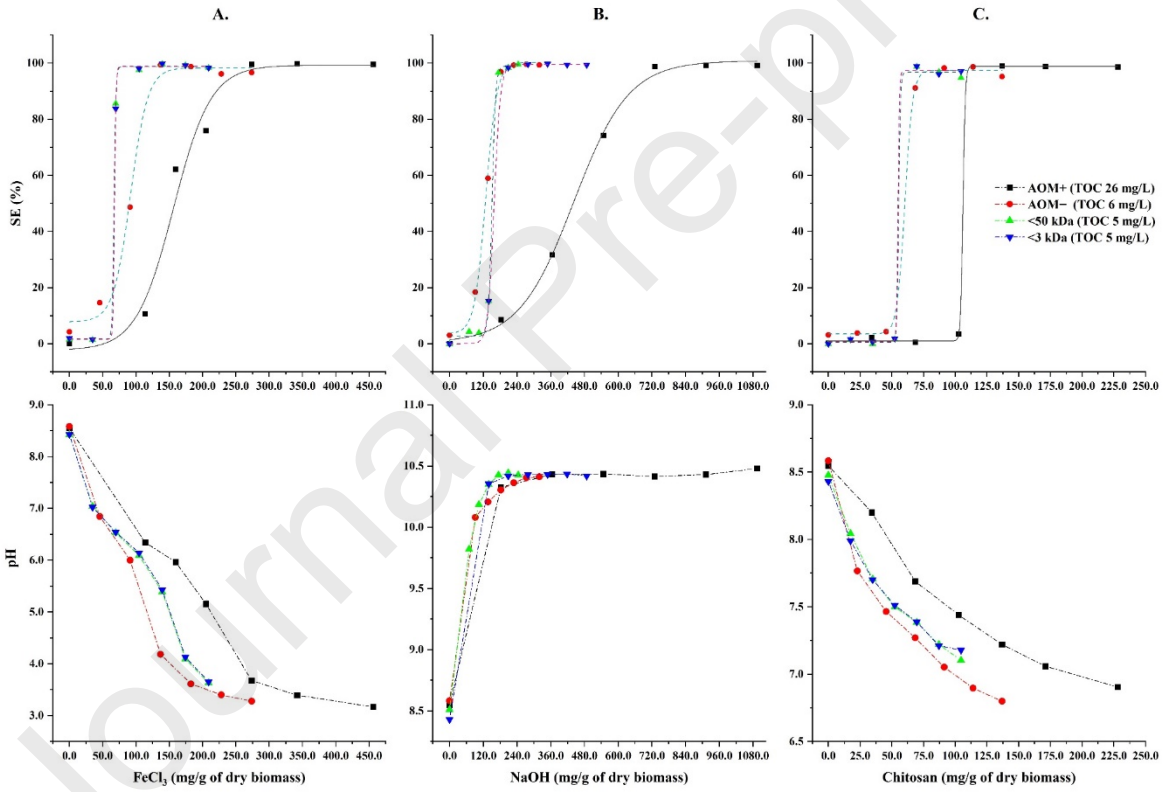

Figure 4: First row: Dose-response curves (SE% corresponding to an applied dosage of **A.** $FeCl_3$, **B.** NaOH, and **C.** Chitosan) from sigmoidal regression of resuspension jar tests with AOM permeate fractions (Jar test set 2). Second row: Final pH values corresponding to applied dosages. For each sigmoidal regression, R^2 = 1.00.

The most critical observation is the approximately synchronized dose responses of <50 kDa and <3 kDa AOM culture suspensions with the AOM− culture. Except for the subtle variation in $FeCl_3$ flocculation of AOM− culture, the dose-response and pH change trajectories

followed a consistent pattern. This observation indicates that low to medium MW (<3 kDa and <50 kDa) AOM fractions are less likely to be primary contributors to flocculation inhibition. Low TOC contents (5–6 $mg \cdot L^{-1}$) of AOM−, <50 kDa and <3 kDa AOM culture suspensions support the synchronizing dose-response curves, in contrast to AOM+ culture (26 $mg \cdot L^{-1}$). Thus, the majority of the flocculation–inhibiting substances are likely in the high MW (>50 kDa) AOM fraction. To confirm this hypothesis, further jar tests (set 3) were carried out with the concentrated AOM retentate fraction.

3.4 Interference of AOM retentate fraction in flocculation (Jar test set 3)

Two different concentrated AOM retentate fractions (~0.7 L each) of >50 kDa (high MW) and 3–50 kDa (medium MW) were obtained after the sequential ultrafiltration. Since jar test set 2 demonstrated that <50 kDa AOM fraction is not primarily responsible for flocculation inhibition, detailed jar tests with 3–50 kDa AOM retentate fraction were not included (also confirmed with preliminary jar tests, data not included). Thus, jar tests (set 3) were carried out only with >50 kDa AOM retentate fraction. AOM− culture control tests achieved SE of ≥ 98% for each flocculant at a given optimum dosage, with corresponding pH of 3.5, 10.5, and 7.1 for $FeCl_3$, NaOH, and chitosan, respectively (Figure 5). SE (≥ 98%) remained unaffected till the addition of >50 kDa AOM up to 5 $mg \cdot L^{-1}$ (TOC equivalent concentration). However, with increasing concentration of >50 kDa AOM, SE decreased for all three flocculants. Flocculation by chitosan was impacted most with complete inhibition (SE reduced to 2%), followed by NaOH (14%) and $FeCl_3$ (34%) at a TOC concentration of 33 $mg \cdot L^{-1}$. This TOC level can typically be reached in early stationary phase culture (Figure 2B). The flocculation inhibition effect can be alleviated by increasing the flocculant dosage; however, complete restoration of SE (≥ 98%) was not observed at the given final flocculant dosages (increased SE % for the final treatment, open symbols above dashed arrow, Figure 5). The final pH after increased dosing did not change significantly. From the AOM fractions jar tests (sets 2 and 3), it is clear that high MW >50 kDa AOM fraction is primarily accountable for flocculation interference, demanding higher flocculant dosage. Such inhibition by higher MW AOM has also been suggested in previous studies by Bernhardt et al.(>2 kDa) (Bernhardt et al., 1991), Vandamme et al. (>3 kDa) (Vandamme et al., 2016), Takaara et al.(>10 kDa) (Takaara et al., 2010), and Yang (>50 kDa) (Yang et al., 2020).

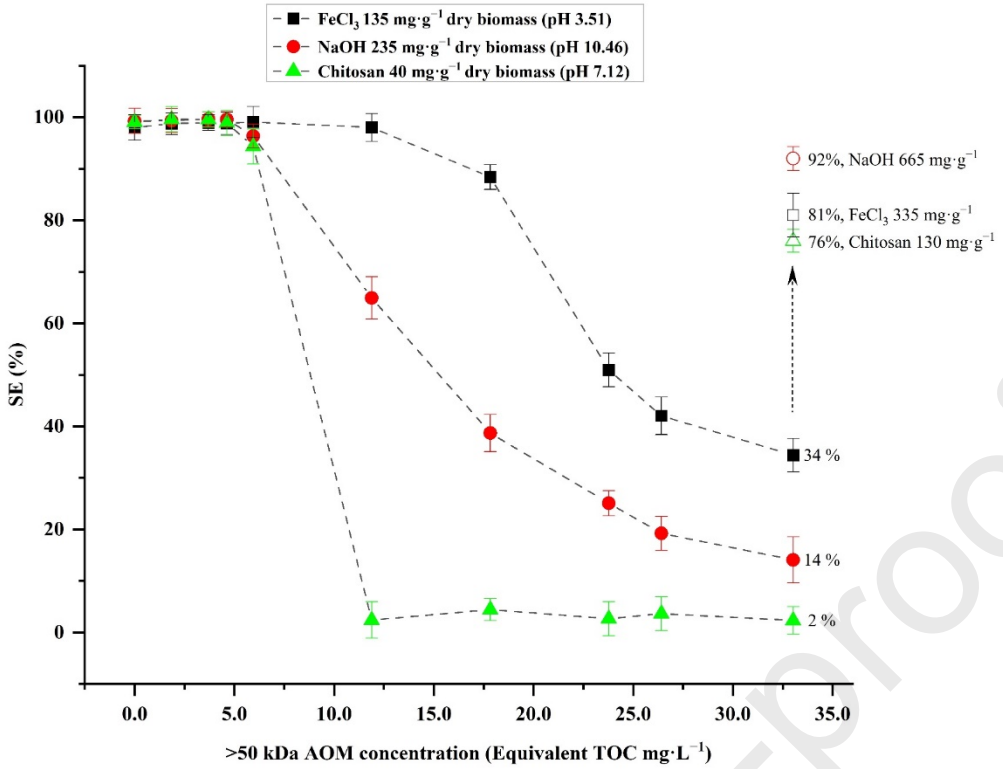

Figure 5: Dose-response (SE %) at increasing concentrations of >50 kDa AOM fraction using optimum flocculant dosage in AOM− culture (resuspension jar test set 3). Individually labeled SE % for the final treatment (open symbols above dashed arrow) represents the increased SE after adding extra flocculant dosage up to the final concentration, as mentioned in the data points.

As observed from the jar test series, AOM demands a high flocculant dosage, suggesting an interaction between flocculants and AOM (Fan et al., 2017; Pivokonsky et al., 2012; Vandamme et al., 2016; Zang et al., 2020; Zhang et al., 2012). This interaction was indirectly assessed by measuring the removal (%) of supernatant TOC, $Fe^{3+,}$ and Mg^{2+} relative to the control culture and AOM (Chen et al., 2009; Fan et al., 2017; Vandamme et al., 2016; Wu et al., 2012). Jar tests were performed on AOM+ culture and AOM only, using optimum flocculant dosages (Table 2). TOC removal was highest for NaOH flocculation. The comparable removal of TOC and Mg^{2+} for both culture and AOM suggests dominant sweep flocculation, which removes both cells and AOM collectively. $FeCl_3$ flocculation showed the lowest TOC removal; however, Fe^{3+} removal was higher in culture (52 %) compared to AOM (29 %). Higher Fe^{3+} removal could be due to the direct/stronger interaction of Fe ions (in cationic hydrolyzed species) with the cells compared to AOM. For chitosan flocculation, TOC removal (%) was calculated after subtracting the TOC contributed by the corresponding chitosan dosage, and the removal was higher than that observed for $FeCl_3$. In general, the removal of TOC/flocculant is varied broadly, indicating different mechanisms and degrees of interaction. Therefore, to discern the interaction dynamics of AOM and different flocculants, it is crucial to analyze the AOM composition and their major active functional groups in the given physiochemical environment (pH, salinity, ionic strength, etc.) (Henderson et al., 2008; Pivokonsky et al., 2012; Zang et al., 2020; Zhang et al., 2012).

Table 2: Jar test supernatant flocculant-AOM removal (%) measured in terms of TOC, Fe^{3+}, and Mg^{2+}.

Treatments*	Supernatant TOC removal (%)	Supernatant Fe^{3+} or Mg^{2+} removal (%)	SE (%)
AOM+ culture + $FeCl_3$	15	52	89
AOM+ culture + NaOH	64	58	98
AOM+ culture + Chitosan	62	NA	98
AOM only + $FeCl_3$	22	29	NA
AOM only + NaOH	67	59	NA
AOM only + Chitosan	49	NA	NA

*Flocculant Dosage: $FeCl_3$ 200 mg·L^{-1}, NaOH 480 mg·L^{-1} (+10 mM Mg^{2+}), Chitosan 75 mg·L^{-1}, Culture dry biomass concentration: 0.60 g·L^{-1}, Culture TOC = 36.5±1.2 mg·L^{-1}, NA: not applicable

3.5 Compositional analysis of AOM retentate (>50 kDa) fraction

AOM interference during flocculation can result from its competition with net negatively charged cells for positively charged flocculants or from complex formation, depending on AOM composition (Cheng et al., 2022; Naveed et al., 2019; Pivokonsky et al., 2012; Zang et al., 2020). The >50 kDa AOM fraction, primarily responsible for flocculation inhibition, was characterized using FTIR and NMR, providing detailed compositional and structural information without altering the sample. Subsequently, acid-hydrolyzed AOM was used for monosaccharide composition analysis using HPAEC–PAD.

3.5.1 FTIR analysis of >50 kDa AOM fraction

The FTIR spectrum of >50 kDa AOM revealed characteristics indicative of abundant polysaccharides, as evidenced by intense bands in the 1200–900 cm^{-1} region (Figure 6A) (Barborikova et al., 2019; Cybulska et al., 2016; Liu et al., 2021). A broad band around 3296 cm^{-1}, encompassing both O–H and N–H stretching, along with aliphatic sidechain CH_2 stretching at 2933 cm^{-1}, is typical of hydrophilic polysaccharides (Barborikova et al., 2019; Cybulska et al., 2016; Villacorte et al., 2015). A major peak at 1039 cm^{-1} denotes C–O stretch and C–O–H in-plane bending vibrations of the pyranose ring in the polysaccharide (Cybulska et al., 2016). A small peak at 897 cm^{-1} suggests β configuration (C1–H bending) of glycosidic

linkages. The bands in the region 735–450 cm^{-1} represent C–C stretch skeletal vibrations (Liu et al., 2021).

A sharp peak at 1248 cm^{-1} signifies the key properties of polysaccharides from the bending vibrations of C–O–H and C–C in carboxylic acid/ester moieties. Two small peaks at 1373 cm^{-1} and 1414 cm^{-1} represent the bending and wagging of CH and CH_2 groups of polysaccharides, respectively. A relatively broad peak in the region 1656–1536 cm^{-1} is characteristic of carboxylate C=O and N–H deformations of amide I/II of glycan N–acetyl groups and protein secondary structure. Since >50 kDa AOM is richer in carbohydrates (42 wt.%) than proteins (23 wt. %), the amide I/II bands are plausibly due to the glycoprotein nature of the AOM.

The prominent peak at 1728 cm^{-1} indicates the C=O stretch of the protonated carboxylic group (–COOH) from uronic acids (Capek et al., 2008). This unique –COOH peak is absent in 3–50 kDa AOM fraction (see supplementary material, Figure S1), aligning with the jar test (set 2) observation that there was no flocculation inhibition in <50 kDa AOM resuspension culture (Figure 4). In contrast, inhibition was clearly observed (jar test set 3) with >50 kDa AOM containing –COOH peak (Figure 5). Overall, >50 kDa AOM is a complex glycan with a unique presence of carboxyl–bearing uronic or sialic acids (Capek et al., 2008; Pinel et al., 2020).

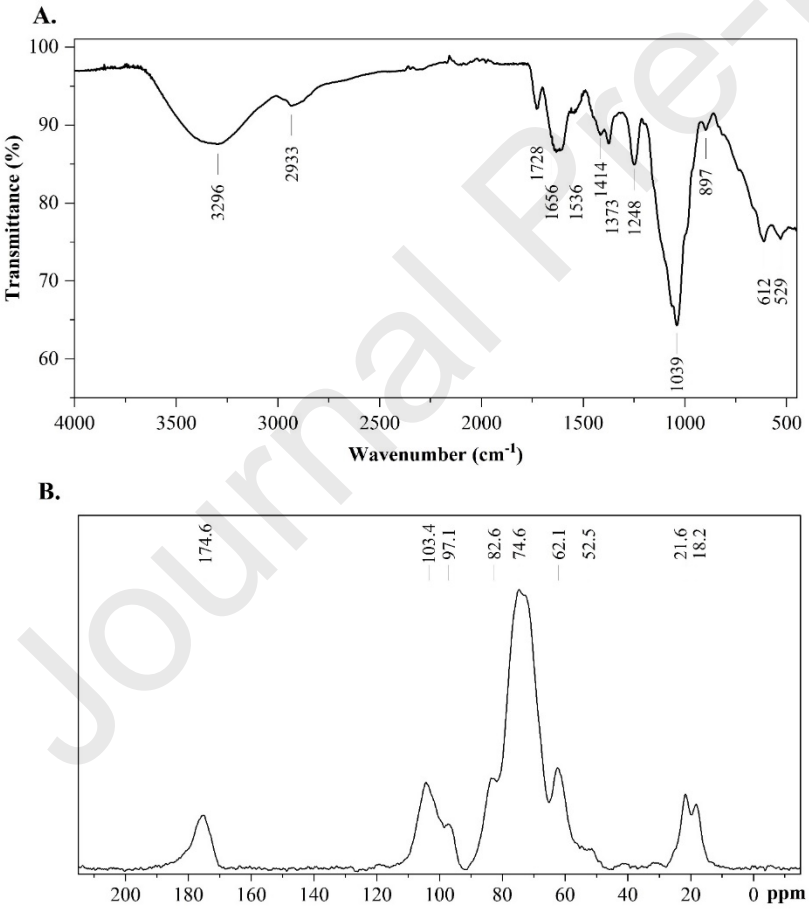

Figure 6: A. FTIR spectrum and **B.** ^{13}C-CP/MAS NMR spectrum of >50 kDa AOM fraction.

3.5.2 *Solid–state ^{13}C-NMR spectroscopy analysis of >50 kDa AOM fraction*

The ^{13}C–CP/MAS NMR spectrum of >50 kDa AOM is shown in Figure 6B**.** The broad resonance signals in the 60–110 ppm range originate from the different carbon units (C1–C6) of hexose sugar, indicating the presence of high MW glycans (Capek et al., 2008). A conspicuous signal at 174.6 ppm is attributed to carbonyl carbons (C=O) from N–acetylamino groups as well as to the carboxylic acid (–**C**OOH) functional group of uronic and sialic acid monomer units in glycan (Arnold et al., 2015; Capek et al., 2008; Kang et al., 2018; Perez Garcia et al., 2011). A peak at 103.4 ppm corresponds to the β–anomeric carbons (C1) involved in glycosidic linkages (O–C–O functionalities) of monomer units such as glucose and galactose. A small shoulder peak at 97.1 represents α–anomeric C1 carbons from monomer units such as xylose, rhamnose, galacturonic acid, etc. (Arnold et al., 2015; Perez Garcia et al., 2011; White et al., 2014).

A broad peak between 60–85 ppm covers the different carbon units (C2, C3, C4, C5, and C6) of the monomer units (Perez Garcia et al., 2011; Poulhazan et al., 2021). An intense peak at 74.6 ppm corresponds to the C2/C5 carbons, with a shoulder peak at 82.6 ppm due to C3/C4 carbons. The distinct peak at 62.1 ppm arises due to hydroxymethyl carbons **C**H_2OH (C6). A small indistinct shoulder signal at 52.5 ppm can be attributed to a methoxyl carbon (–CO**OC**$\mathbf{H_3}$), such as the ester methoxy group attached to carbonyl carbon (C6) of galacturonic acid. The peaks in the 15–36 ppm region are generally assigned to aliphatic sidechains (CH_3, CH_2, and CH) of lipids and proteins (Poulhazan et al., 2021; White et al., 2014). However, absence of strong signals from sp^2 hybridized carbon in the region 110–160 ppm (due to aromatic amino acids and unsaturated C=C bonds in lipids and fatty acids) implies that the aliphatic signals are most likely from methyl carbons (**C**H_3) of glycan monomers (Capek et al., 2008; Mathieu-Rivet et al., 2020; Perez Garcia et al., 2011; Poulhazan et al., 2021).

A peak at 21.6 ppm (combined with the carbonyl (C=O) peak at 174.6 ppm) can be assigned to methyl carbons from acetyl groups (–CO**C**$\mathbf{H_3}$), such as the acetyl CH_3 of N–acetylglucosamine. Generally, the core of N–glycans contains two residues of N–acetylglucosamine, which, along with other residues in the glycan structure, could be the origin of the acetyl CH_3 signal (Capek et al., 2008; Mathieu-Rivet et al., 2020; Perez Garcia et al., 2011; White et al., 2014). The small shoulder at 18.2 ppm represents the methyl carbons (–**C**H_3) from 6–deoxy sugars (e.g., C6 of rhamnose and fucose) (Capek et al., 2008; White et al., 2014). Thus, >50 kDa AOM fraction is a high MW complex glycan with carboxyl (–COOH) and N–acetylamino (-NHCOCH_3) group-bearing monomers.

3.5.3 Total carbohydrate, total protein, and monosaccharides composition of >50 kDa AOM fraction

The total carbohydrate and protein contents of >50 kDa AOM were 42% and 23% on a lyophilized dry weight basis (wt %), respectively, indicating its glycoprotein nature (Capek et al., 2008; Rao et al., 2020). Moisture and ash content were 6 wt % and 9 wt %, as determined via thermogravimetric analysis. HPAEC–PAD-based analysis of monosaccharides after acid hydrolysis shows that the AOM is a heteropolysaccharide composed of neutral, amino, and acidic sugars (see supplementary material, Figure S2). Quantified monosaccharides consisted of arabinose (30.05 wt %), glucosamine (6.58 wt %), glucose (4.17 wt %), xylose (3.02 wt %), mannose (3.81 wt %), and glucuronic acid (1.75 wt %). Trace amounts of rhamnose (retention time, RT–9.8 min) and galactose were detected but not quantified due to the low peak area. Fucose and ribose were not present in the AOM. One small peak in the neutral sugar region (RT–11.7 min) was not identified. In addition to traces of galacturonic acid, a

major unidentified peak in the acidic sugar region (RT–35.8 min) is most likely of N–acetylneuraminic acid (Neu5Ac), a prominent sialic acid typically present as a terminal sugar in the glycoprotein complexes (Capek et al., 2008; Cybulska et al., 2016; Mathieu-Rivet et al., 2020; Pinel et al., 2020). The presence of acidic sugars confirms the carboxyl functional groups (–COOH) in the AOM, which were also detected in the FTIR and ^{13}C–CP/MAS NMR spectra.

3.6 Potential functional group(s) responsible for flocculation inhibition based on the compositional analysis

Overall compositional analyses of >50 kDa AOM fraction illustrated that it is a high MW heteropolysaccharide composed of neutral, amino, and acidic sugars. Among various functional groups, the carboxyl group (–COOH) from acidic monomers– prominently observed in this study– is particularly important from the flocculation perspective. The interaction of surface-active carboxyl groups with cationic flocculants could occur through ion exchange, complexion, or precipitation (Kaplan et al., 1987; Naveed et al., 2019). Thus, competition between cell–surface and AOM carboxyl groups for the flocculant, leading to a higher dosage requirement, is a well-observed phenomenon in this and other studies (Brady et al., 2014; Cheng et al., 2022; Pivokonsky et al., 2012; Vandamme et al., 2016; Zang et al., 2020; Zhang et al., 2012).

A recent study by Cheng *et al.* suggested a low suspension pH to prevent the deprotonation of the carboxyl group to reduce the inhibitory effect of carboxyl groups (Cheng et al., 2022). In this study, even though the optimum pH was in the acidic range (2.70–3.45 at maximum SE %) for $FeCl_3$ flocculation, the AOM inhibitory effect was still present (Figures 3 and 4), indicating strong inhibitory effects of the carboxyl group. In comparison, a much higher inhibitory effect was observed for the NaOH flocculation at pH 10.5. At alkaline pH, deprotonated carboxyl groups of AOM may chelate Mg^{2+} ions, demanding higher NaOH dosages to induce $Mg(OH)_2$ precipitate formation (Besson & Guiraud, 2013; Brady et al., 2014; Vandamme et al., 2016). Additionally, deprotonated phosphoryl and hydroxyl groups could amplify Mg^{2+}chelation, inducing a stronger inhibitory effect compared to acidic pH conditions in $FeCl_3$ flocculation (Figures 3, 4, and 5) (Besson & Guiraud, 2013; Fan et al., 2017; Vandamme et al., 2016; Wu et al., 2012). Moreover, the optimum chitosan flocculation (SE ≥98 %) occurred in the neutral pH region (6.25–7.25, Figures 3 and 4), where carboxyl groups (pK_a 2–6) mostly remained deprotonated (Pivokonsky et al., 2012). The strong polarity of the deprotonated carboxyl groups can induce high electrostatic interactions (coordinate bonds) with positively charged amine ($–NH_3^+$) functional groups of chitosan (pK_a ~ 6.5) (Zang et al., 2020). This could explain the significantly higher inhibition tendency of chitosan by >50 kDa AOM compared to $FeCl_3$ or NaOH flocculation (Figure 5).

For all the flocculants used in this study, AOM interference was due to a high MW (>50 kDa) fraction. Thus, interfering functional groups such as carboxyl, phosphoryl, amine, and hydroxyl should be associated with the polysaccharide complex rather than small MW oligo– or monosaccharides. Studies on model AOM demonstrated that only the polymeric molecule (alginate), not the monosaccharides, had an inhibitory effect on flocculation (Beuckels et al., 2013; Cheng et al., 2022; Vandamme et al., 2016). In this study, AOM used mainly comprised cell-secreted soluble extracellular organic matter. Generally, as in other microorganisms, microalgal extracellular organic matter is also secreted as a glycoconjugate complex performing various cellular functions such as substrate adhesion, nutrient retention, and protection against dehydration, predatory microbes or harmful chemicals, etc. (Mathieu-Rivet et al., 2020; Rao et al., 2020; Zhou et al., 2024). Most of this secreted extracellular

matter consists of glycoproteins with diverse compositions and proportions of glycan monomer (Mathieu-Rivet et al., 2020; Rao et al., 2020). Based on the total carbohydrate/protein and monosaccharide compositions in this study, it is conceivable that the AOM is structured as a glycoprotein, potentially featuring either N–glycan with xylosylated core (N–acetylglucosamine2, Man3) or O–glycan with sialic acid terminal (Capek et al., 2008; Mathieu-Rivet et al., 2020; Pinel et al., 2020; Rao et al., 2020). Thus, further studies on glycosidic linkage and glycoprotein genomics/proteomics are needed to elucidate the AOM structure and the conformational state of active functional groups interfering with the flocculation process.

4 Conclusion

This study demonstrates that the >50 kDa AOM fraction is primarily responsible for the inhibition of *Chlorella* sp. flocculation induced by $FeCl_3$, NaOH, and chitosan., requiring increased flocculant dosages. The presence of carboxyl groups (–COOH) from acidic monomers in AOM plays a crucial role in this inhibition, particularly under varying pH conditions. Compositional analysis confirmed that AOM is a high MW glycoprotein rich in carbohydrates. These findings highlight the importance of understanding AOM composition and interactions with flocculants to optimize flocculation processes. Further research on glycosidic linkages and glycoprotein structures is recommended to mitigate AOM's inhibitory effects.

References:

1. Ajala, S.O., Alexander, M.L. 2020. Assessment of *Chlorella vulgaris*, *Scenedesmus obliquus*, and *Oocystis minuta* for removal of sulfate, nitrate, and phosphate in wastewater. *International Journal of Energy and Environmental Engineering*, **11**(3), 311-326.

2. Arnold, A.A., Genard, B., Zito, F., Tremblay, R., Warschawski, D.E., Marcotte, I. 2015. Identification of lipid and saccharide constituents of whole microalgal cells by (1)(3)C solid-state NMR. *Biochim Biophys Acta*, **1848**(1 Pt B), 369-77.

3. Barborikova, J., Sutovska, M., Kazimierova, I., Joskova, M., Franova, S., Kopecky, J., Capek, P. 2019. Extracellular polysaccharide produced by *Chlorella vulgaris* - Chemical characterization and anti-asthmatic profile. *Int J Biol Macromol*, **135**, 1-11.

4. Bernhardt, H., Schell, H., Hoyer, O., Lüsse, B. 1991. Influence of algogenic organic substances on flocculation and filtration. *WISA*. pp. 41-57.

5. Besson, A., Guiraud, P. 2013. High-pH-induced flocculation-flotation of the hypersaline microalga *Dunaliella salina*. *Bioresour Technol*, **147**, 464-470.

6. Beuckels, A., Depraetere, O., Vandamme, D., Foubert, I., Smolders, E., Muylaert, K. 2013. Influence of organic matter on flocculation of *Chlorella vulgaris* by calcium phosphate precipitation. *Biomass and Bioenergy*, **54**, 107-114.

7. Brady, P.V., Pohl, P.I., Hewson, J.C. 2014. A coordination chemistry model of algal autoflocculation. *Algal Research*, **5**(1), 226-230.

8. Capek, P., Matulova, M., Combourieu, B. 2008. The extracellular proteoglycan produced by *Rhodella grisea*. *Int J Biol Macromol*, **43**(4), 390-3.

9. Chen, L., Li, P.F., Liu, Z.L., Jiao, Q.C. 2009. The released polysaccharide of the cyanobacterium *Aphanothece halophytica* inhibits flocculation of the alga with ferric chloride. *Journal of Applied Phycology*, **21**(3), 327-331.

10. Cheng, S., Zhang, H., Li, L., Yu, T., Wang, Y., Tan, D., Zhang, X. 2022. Harvesting of *Microcystis flos-aquae* using dissolved air flotation: The inhibitory effect of carboxyl groups in uronic acid-containing carbohydrates. *Chemosphere*, **300**, 134466.

11. Cheng, S., Zhang, H., Wang, H., Mubashar, M., Li, L., Zhang, X. 2024. Influence of algal organic matter in the in-situ flotation removal of Microcystis using positively charged bubbles. *Bioresour Technol*, **397**, 130468.

12. Cybulska, J., Halaj, M., Cepák, V., Lukavsky, J., Capek, P. 2016. Nanostructure features of microalgae biopolymer. *Starch-Starke*, **68**(7-8), 629-636.

13. Demir, I., Blockx, J., Dague, E., Guiraud, P., Thielemans, W., Muylaert, K., Formosa-Dague, C. 2020. Nanoscale Evidence Unravels Microalgae Flocculation Mechanism Induced by Chitosan. *ACS Appl Bio Mater*, **3**(12), 8446-8459.

14. Fan, J., Zheng, L., Bai, Y., Saroussi, S., Grossman, A.R. 2017. Flocculation of *Chlamydomonas reinhardtii* with Different Phenotypic Traits by Metal Cations and High pH. *Front Plant Sci*, **8**, 1997.

15. Garzon-Sanabria, A.J., Ramirez-Caballero, S.S., Moss, F.E., Nikolov, Z.L. 2013. Effect of algogenic organic matter (AOM) and sodium chloride on *Nannochloropsis salina* flocculation efficiency. *Bioresour Technol*, **143**, 231-7.

16. Henderson, R., Parsons, S.A., Jefferson, B. 2008. The impact of algal properties and pre-oxidation on solid-liquid separation of algae. *Water Res*, **42**(8-9), 1827-45.

17. Johnson, P.N., Amirtharajah, A. 1983. Ferric chloride and alum as single and dual coagulants. *Journal AWWA*, **75**(5), 232-239.

18. Kang, X., Kirui, A., Muszynski, A., Widanage, M.C.D., Chen, A., Azadi, P., Wang, P., Mentink-Vigier, F., Wang, T. 2018. Molecular architecture of fungal cell walls revealed by solid-state NMR. *Nat Commun*, **9**(1), 2747.

19. Kaplan, D., Christiaen, D., Arad, S.M. 1987. Chelating Properties of Extracellular Polysaccharides from *Chlorella* spp. *Appl Environ Microbiol*, **53**(12), 2953-6.

20. Kim, D.Y., Oh, Y.K., Park, J.Y., Kim, B., Choi, S.A., Han, J.I. 2015. An integrated process for microalgae harvesting and cell disruption by the use of ferric ions. *Bioresour Technol*, **191**, 469-74.

21. Lama, S., Muylaert, K., Karki, T.B., Foubert, I., Henderson, R.K., Vandamme, D. 2016. Flocculation properties of several microalgae and a cyanobacterium species during ferric chloride, chitosan and alkaline flocculation. *Bioresour Technol*, **220**, 464-470.

22. Li, Y.F., Ma, Q.W., Pan, Y.W., Chen, Q.X., Sun, Z.T., Hu, P. 2021. Development of an effective flocculation method by utilizing the auto-flocculation capability of *Phaeodactylum tricornutum*. *Algal Research-Biomass Biofuels and Bioproducts*, **58**, 102413-102413.

23. Liu, X., Renard, C., Bureau, S., Le Bourvellec, C. 2021. Revisiting the contribution of ATR-FTIR spectroscopy to characterize plant cell wall polysaccharides. *Carbohydr Polym*, **262**, 117935.

24. Liu, Z., Hao, N., Hou, Y., Wang, Q., Liu, Q., Yan, S., Chen, F., Zhao, L. 2023. Technologies for harvesting the microalgae for industrial applications: Current trends and perspectives. *Bioresour Technol*, **387**, 129631.

25. Mathieu-Rivet, E., Mati-Baouche, N., Walet-Balieu, M.L., Lerouge, P., Bardor, M. 2020. N- and O-Glycosylation Pathways in the Microalgae Polyphyletic Group. *Front Plant Sci*, **11**, 609993.

26. McGrath, S.J., Laamanen, C.A., Senhorinho, G.N.A., Scott, J.A. 2024. Microalgal harvesting for biofuels – Options and associated operational costs. *Algal Research*, **77**, 103343-103343.

27. Nagel, A., Sirisakulwat, S., Carle, R., Neidhart, S. 2014. An acetate-hydroxide gradient for the quantitation of the neutral sugar and uronic acid profile of pectins by HPAEC-PAD without postcolumn pH adjustment. *J Agric Food Chem*, **62**(9), 2037-48.

28. Naveed, S., Li, C.H., Lu, X.D., Chen, S.S., Yin, B., Zhang, C.H., Ge, Y. 2019. Microalgal extracellular polymeric substances and their interactions with metal(loid)s: A review. *Critical Reviews in Environmental Science and Technology*, **49**(19), 1769-1802.

29. Perez Garcia, M., Zhang, Y., Hayes, J., Salazar, A., Zabotina, O.A., Hong, M. 2011. Structure and interactions of plant cell-wall polysaccharides by two- and three-dimensional magic-angle-spinning solid-state NMR. *Biochemistry*, **50**(6), 989-1000.

30. Pinel, I.S.M., Kleikamp, H.B.C., Pabst, M., Vrouwenvelder, J.S., van Loosdrecht, M.C.M., Lin, Y.M. 2020. Sialic Acids: An Important Family of Carbohydrates Overlooked in Environmental Biofilms. *Applied Sciences-Basel*, **10**(21), 7694-7694.

31. Pivokonsky, M., Safarikova, J., Bubakova, P., Pivokonska, L. 2012. Coagulation of peptides and proteins produced by *Microcystis aeruginosa*: Interaction mechanisms and the effect of Fe-peptide/protein complexes formation. *Water Res*, **46**(17), 5583-5590.

32. Poulhazan, A., Dickwella Widanage, M.C., Muszynski, A., Arnold, A.A., Warschawski, D.E., Azadi, P., Marcotte, I., Wang, T. 2021. Identification and Quantification of Glycans in Whole Cells: Architecture of Microalgal Polysaccharides Described by Solid-State Nuclear Magnetic Resonance. *J Am Chem Soc*, **143**(46), 19374-19388.

33. Qin, S., Wang, K., Gao, F., Ge, B., Cui, H., Li, W. 2023. Biotechnologies for bulk production of microalgal biomass: from mass cultivation to dried biomass acquisition. *Biotechnol Biofuels Bioprod*, **16**(1), 131.

34. Rao, N.R.H., Granville, A.M., Wich, P.R., Henderson, R.K. 2020. Detailed algal extracellular carbohydrate-protein characterisation lends insight into algal solid-liquid separation process outcomes. *Water Res*, **178**, 115833.

35. Shitanaka, T., Fujioka, H., Khan, M., Kaur, M., Du, Z.Y., Khanal, S.K. 2024. Recent advances in microalgal production, harvesting, prediction, optimization, and control strategies. *Bioresour Technol*, **391**(Pt A), 129924.

36. Takaara, T., Sano, D., Masago, Y., Omura, T. 2010. Surface-retained organic matter of *Microcystis aeruginosa* inhibiting coagulation with polyaluminum chloride in drinking water treatment. *Water Res*, **44**(13), 3781-6.

37. Van Wychen, S., Laurens, L.M.L. 2016. Determination of Total Carbohydrates in Algal Biomass: Laboratory Analytical Procedure (LAP).

38. Vandamme, D., Beuckels, A., Vadelius, E., Depraetere, O., Noppe, W., Dutta, A., Foubert, I., Laurens, L., Muylaert, K. 2016. Inhibition of alkaline flocculation by algal organic matter for *Chlorella vulgaris*. *Water Res*, **88**, 301-307.

39. Vandamme, D., Foubert, I., Fraeye, I., Muylaert, K. 2012. Influence of organic matter generated by *Chlorella vulgaris* on five different modes of flocculation. *Bioresour Technol*, **124**, 508-11.

40. Villacorte, L.O., Ekowati, Y., Neu, T.R., Kleijn, J.M., Winters, H., Amy, G., Schippers, J.C., Kennedy, M.D. 2015. Characterisation of algal organic matter produced by bloom-forming marine and freshwater algae. *Water Res*, **73**, 216-30.

41. Vu, H.P., Nguyen, L.N., Emmerton, B., Wang, Q., Ralph, P.J., Nghiem, L.D. 2021. Factors governing microalgae harvesting efficiency by flocculation using cationic polymers. *Bioresour Technol*, **340**, 125669.

42. White, P.B., Wang, T., Park, Y.B., Cosgrove, D.J., Hong, M. 2014. Water-polysaccharide interactions in the primary cell wall of *Arabidopsis thaliana* from polarization transfer solid-state NMR. *J Am Chem Soc*, **136**(29), 10399-409.

43. Wu, Z., Zhu, Y., Huang, W., Zhang, C., Li, T., Zhang, Y., Li, A. 2012. Evaluation of flocculation induced by pH increase for harvesting microalgae and reuse of flocculated medium. *Bioresour Technol*, **110**(SUPPL.2), 496-502.

44. Wyatt, N.B., Gloe, L.M., Brady, P.V., Hewson, J.C., Grillet, A.M., Hankins, M.G., Pohl, P.I. 2012. Critical conditions for ferric chloride-induced flocculation of freshwater algae. *Biotechnol Bioeng*, **109**(2), 493-501.

45. Yang, L., Zhang, H.Y., Cheng, S.Z., Zhang, W., Zhang, X.Z. 2020. Enhanced Microalgal Harvesting Using Microalgae-Derived Extracellular Polymeric Substance as Flocculation Aid. *Acs Sustainable Chemistry & Engineering*, **8**(10), 4069-4075.

46. Zang, X., Zhang, H., Liu, Q., Li, L., Li, L., Zhang, X. 2020. Harvesting of *Microcystis flos-aquae* using chitosan coagulation: Influence of proton-active functional groups originating from extracellular and intracellular organic matter. *Water Res*, **185**, 116272.

47. Zhang, S., Cao, J., Zheng, Y., Hou, M., Song, L., Na, J., Jiang, Y., Huang, Y., Liu, T., Wei, H. 2024. Insight into coagulation/flocculation mechanisms on microalgae harvesting by ferric chloride and polyacrylamide in different growth phases. *Bioresour Technol*, **393**, 130082.

48. Zhang, X., Amendola, P., Hewson, J.C., Sommerfeld, M., Hu, Q. 2012. Influence of growth phase on harvesting of *Chlorella zofingiensis* by dissolved air flotation. *Bioresour Technol*, **116**, 477-84.

49. Zhou, Y., Cui, X., Wu, B., Wang, Z., Liu, Y., Ren, T., Xia, S., Rittmann, B.E. 2024. Microalgal extracellular polymeric substances (EPS) and their roles in cultivation, biomass harvesting, and bioproducts extraction. *Bioresour Technol*, **406**, 131054.

CRediT authorship contribution statement

Sanjaya Lama: Conceptualization, Methodology, Investigation, Formal analysis, Data curation, Visualization, Writing – original draft. **Michaela Pappa:** Methodology, Investigation, Writing – review & editing. **Nathalia Brandão Watanabe**: Investigation. **Cécile Formosa–Dague:** Funding acquisition, Methodology, Writing – review & editing. **Wouter Marchal:** Funding acquisition, Resources, Methodology, Supervision, Writing – review & editing. **Peter Adriaensens:** Funding acquisition, Resources, Methodology, Supervision, Writing – review & editing. **Dries Vandamme:** Funding acquisition, Resources, Methodology, Visualization, Validation, Supervision, Writing – review & editing.

Declaration of interests

☒ The authors declare that they have no known competing financial interests or personal relationships that could have appeared to influence the work reported in this paper.

☐ The authors declare the following financial interests/personal relationships which may be considered as potential competing interests:

Graphical Abstract

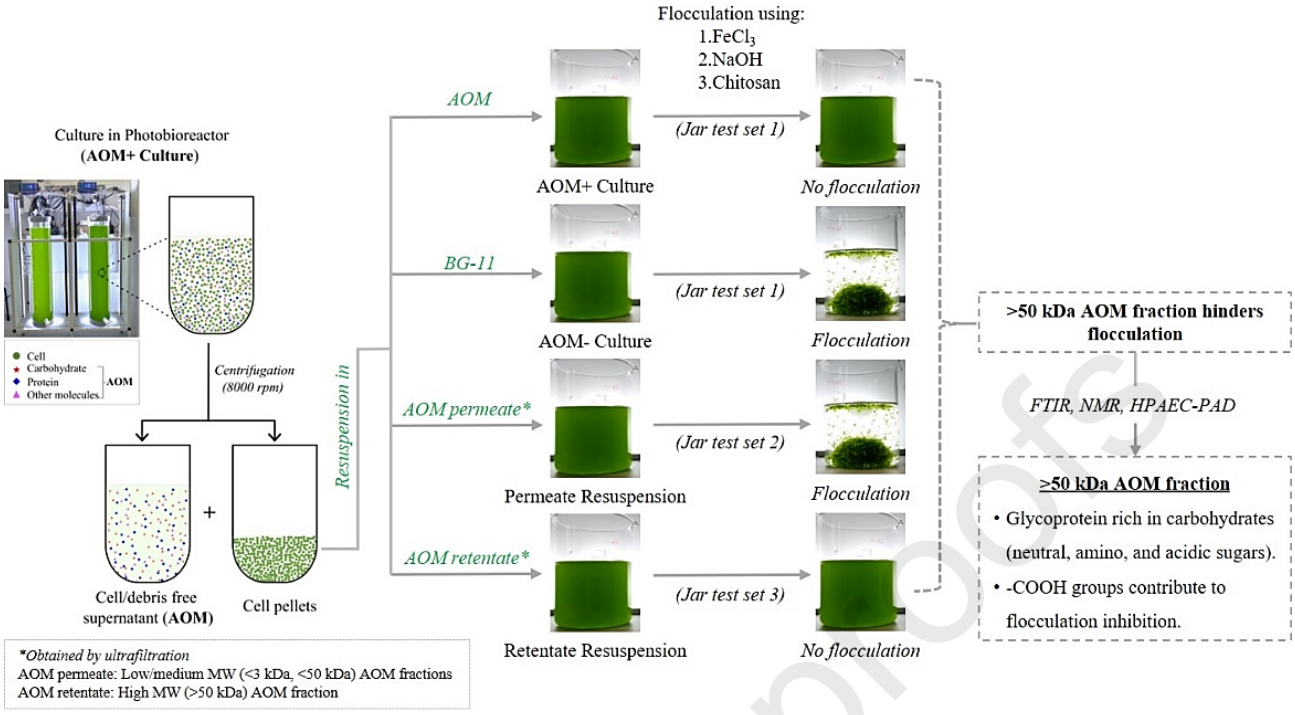

Highlights

- AOM increased flocculant dosage requirement for effective microalgae harvesting.
- High molecular weight (>50 kDa) AOM fraction inhibited flocculation.
- FTIR and NMR identified carbohydrate-rich glycoprotein in >50 kDa AOM fraction.
- -COOH groups from acidic monomers of >50 kDa AOM contribute to inhibitory action.